Title

Simulated Sea Level Rise in Coastal Peat Soils Stimulates Mercury Methylation

Authors

Cook, Bryce A

Peterson, Benjamin D

Ogorek, Jacob M

et al.

Publication Date

2024

DOI

10.1021/acsearthspacechem.4c00124

Peer reviewed

ACS EARTH AND SPACE CHEMISTRY

Editors' Choice
Open Access

http://pubs.acs.org/journal/aesccq

Article

Simulated Sea Level Rise in Coastal Peat Soils Stimulates Mercury Methylation

Bryce A. Cook, Benjamin D. Peterson, Jacob M. Ogorek, Sarah E. Janssen, and Brett A. Poulin*

Cite This: https://doi.org/10.1021/acsearthspacechem.4c00124

Read Online

ACCESS | Metrics & More | Article Recommendations | Supporting Information

ABSTRACT: Coastal wetlands are vulnerable to sea level rise with unknown consequences for mercury (Hg) cycling, particularly the potential for exacerbating neurotoxic methylmercury (MeHg) production and bioaccumulation in food webs. Here, the effect of sea level rise on MeHg formation in the Florida Everglades was evaluated by incubating peat cores from a freshwater wetland for 0−20 days in the laboratory at five salinity conditions (0.16−6.0 parts-per-thousand; 0.20−454 mg L^{-1} sulfate (SO_4^{2-})) to simulate the onset of sea level rise within coastal margins. Isotopically enriched inorganic mercury (^{201}Hg(II)) was used to track MeHg formation and peat-porewater partitioning. In all five salinity treatments, porewaters became anoxic within 1 day and became progressively enriched in dissolved organic matter (DOM) of greater aromatic composition over the 20 days compared to ambient conditions. In the four highest salinity treatments, SO_4^{2-} concentrations decreased and sulfide concentrations increased over time due to microbial dissimilatory SO_4^{2-} reduction that was concurrent with ^{201}Hg(II) methylation. Importantly, elevated salinity resulted in a greater proportion of produced Me^{201}Hg observed in porewaters as opposed to bound to peat, interpreted to be due to the complexation of MeHg with aromatic DOM released from peat. The findings highlight the potential for enhanced production and mobilization of MeHg in coastal wetlands of the Florida Everglades due to the onset of saltwater intrusion.

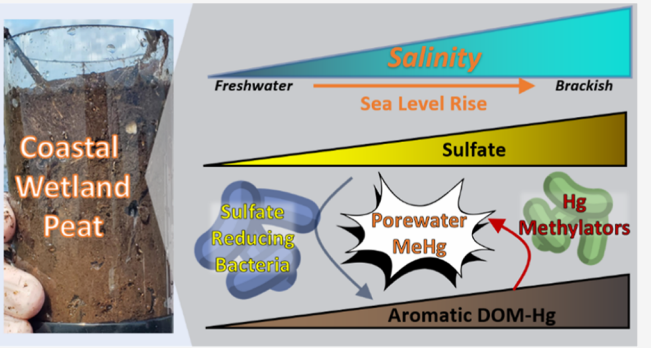

KEYWORDS: *sea level rise, methylmercury, Florida Everglades, peat soils, methylation, sulfate*

INTRODUCTION

Mercury (Hg) is a ubiquitous environmental contaminant that impacts the environment and humans globally.[1] In aquatic environments, inorganic divalent Hg (Hg(II)) can be transformed by microorganisms to neurotoxic methylmercury (MeHg),[2,3] which bioaccumulates in food webs resulting in deleterious health impacts to wildlife and humans.[4] In freshwater and coastal environments, where consumption of fish and shellfish and corresponding exposure to MeHg are known to be greater,[5] perturbations to local biogeochemical processes often control the environmental exposure of wildlife and humans to Hg by mediating the production,[6] fate,[7,8] and transport[9] of MeHg. A body of research on the freshwater Florida Everglades[6,10−12] documents the universal controls of dissolved organic matter (DOM) and sulfate (SO_4^{2-}) on MeHg formation and biological Hg burden.[13] Coastal wetlands, including those in the Florida Everglades, are recognized as locations for DOM[14] and MeHg export to coastal waters due to tidal pumping[9] that can exacerbate the uptake of MeHg in fish.[15] However, a major knowledge gap is the influence of saltwater intrusion and subsequent increases in salinity and specifically SO_4^{2-} on MeHg formation and partitioning in coastal wetlands. Under current projections, up to 97% of coastal wetlands in the U.S. are vulnerable to saltwater intrusion in this century,[16] and seasonal fluctuations in hydrology (i.e., freshwater inputs)[17] and wind- and storm-driven surges[18] can result in dynamic changes in wetland salinity. Thus, there is an urgent need to better understand how this climate-change related disturbance may influence MeHg production and export to neighboring coastal waters.

Sea level rise could have multidimensional effects on the biogeochemical processes that control the formation of MeHg in aquatic environments. Broadly, MeHg formation is governed by the synergy between (1) the potential of the microbial community to methylate Hg(II), which requires the Hg-methylation gene pair (*hgcAB*),[19] and (2) the bioavailability of Hg(II).[2,3,6] Both of these processes are influenced by organic matter composition and lability and SO_4^{2-} concentrations, two key environmental constituents that play many roles in Hg(II)

Received: May 6, 2024
Revised: July 24, 2024
Accepted: July 24, 2024

methylation in diverse wetlands,[10,20−23] estuaries,[24] and freshwater portions of the Florida Everglades.[6,10,23] Sulfate stimulates SO_4^{2-} reducing bacteria, which utilize SO_4^{2-} as a terminal electron acceptor in dissimilatory SO_4^{2-} reduction, fueling anaerobic respiration. The activity of SO_4^{2-} reducing bacteria is recognized as important for MeHg formation in the freshwater Florida Everglades,[10,11,25] despite recent surprising discovery that these organisms do not carry the *hgcAB* gene pair themselves in this ecosystem.[6] Rather, SO_4^{2-} is suspected to stimulate overall microbial metabolism linked to MeHg production through consumption of fermentative products[26] and/or by stimulating methanogenic activity through syntrophy in the Everglades.[6,25,27]

The biogeochemical cycling of SO_4^{2-} is also linked to the enhanced release and production of high molecular weight and aromatic DOM from peat.[28,29] DOM promotes Hg(II) bioavailability for methylation through complexation with DOM thiol moieties[30] and by limiting the formation of nanocolloidal metacinnabar (nano-β-$HgS_{(s)}$) under mildly sulfidic conditions, keeping Hg(II) poorly crystalline[31,32] and suspended in solution.[6,33,34] SO_4^{2-} reduction also increases the concentration of thiol groups in DOM via sulfurization reactions,[35] which directly enhances Hg(II) bioavailability for methylation.[36] Across the freshwater Everglades ecosystem, SO_4^{2-} shows close correspondence with DOM aromaticity,[23,29] quantified by the specific ultraviolet absorbance at 254 nm ($SUVA_{254}$).[37] Further, the effects of SO_4^{2-} on DOM quality and quantity may influence the partitioning of Hg(II) and MeHg from peat sediments to surrounding porewaters,[38] which subsequently could influence MeHg diffusion from peat to the water column and export within coastal regions through tidal pumping.[9] In the Everglades, MeHg enters the food web through accumulation in periphyton and phytoplankton in the water column,[13,15,39,40] thus the solubilizing effects of DOM on the partitioning[41] and tidal export of MeHg[9] are likely a key driver of MeHg bioaccumulation in coastal systems.[15] These biogeochemical controls on MeHg production and fate are well-documented and understood in freshwater and marine wetlands; however, MeHg formation under transient wetland biogeochemical conditions due to sea level rise and the concurrent delivery of seawater SO_4^{2-} is unclear.

Here, we present results of the first microcosm-based evaluation of the influence of saltwater intrusion on MeHg formation in peat cores from freshwater Florida Everglades, an ecosystem particularly susceptible to sea level rise,[42,43] Hg bioaccumulation in fish and marine mammals,[15,23,44] and human Hg exposure.[5] Changes in porewater biogeochemistry and MeHg formation and peat-porewater partitioning were evaluated in intact peat cores incubated at five moderate salinity levels representative of the onset of saltwater intrusion (≤6.0 parts-per-thousand (ppt)). Incubations were conducted for 0−20 days to simulate short-term and long-term shifts in salinity (e.g., tidal cycles vs seasonal fluctuations). We hypothesize that a moderate degree of saltwater intrusion into freshwater peat, and hence intrusion of seawater SO_4^{2-}, would result in increased net MeHg formation due to the aforementioned role of SO_4^{2-} in Hg(II) methylation and bioavailability. These experimental results will provide important context regarding the impacts of sea level rise on MeHg formation, partitioning, and potential export within the coastal Everglades and more broadly to coastal ecosystems worldwide.

METHODS

The Supporting Information provides complete details on the collection of peat cores (Section S1.1), composition of porewater chemistry (Section S1.2), experimental design of laboratory experiments to simulate sea level rise effects (Section S1.3), analyses of water and peat (Section S1.4), and thermodynamic speciation calculations in porewaters (Section S1.5). In brief, peat cores (n = 105 replicates) were collected from a historically low SO_4^{2-} site in Water Conservation Area 3A (WCA-3A, Subsite H)[45,46] of the Florida Everglades (Supporting Information Figure S1) representative of sawgrass-dominated Everglades wetlands currently experiencing sea level rise.[47] Field measurements of the site surface water and porewater were performed (Supporting Information Table S1). The southern Florida Everglades are a particularly at-risk region for sea level rise as approximately half of Everglades National Park lies within 0.6 m of mean sea level[42] with a gradual elevation slope of about 3 cm per lateral km, which poses significant risk for the ecosystem to storm and sea level rise driven inundation. By 2060, sea levels in South Florida are conservatively expected to rise 0.6 m which will cause increases in salinity and inundation in both brackish and freshwater areas of the southern Florida coast.[42]

Laboratory experiments quantified the biogeochemical responses of Hg(II) methylation to saltwater intrusion at moderate salinities in intact Everglades peat between 0 and 20 days. Core flooding experiments were carried out at five salinities (0.16, 0.25, 0.50, 1.0, 6.0 ppt; 0.20−454 mg L^{-1} SO_4^{2-}) (Supporting Information Tables S2−S4), selected based on (1) observed biogeochemical responses related to dissolved organic carbon (DOC) and SO_4^{2-} in previous peat incubations,[48−50] (2) a decadal analysis of SO_4^{2-} and MeHg trends in coastal Everglades National Park,[23] and (3) a temporal analysis of salinity data measured at two sites in coastal Shark River and Shark River Slough of Everglades National Park (Supporting Information Figure S2).[51,52] In the laboratory, peat cores were inundated (Supporting Information Figure S3) with water of uniform DOM chemistry (5.5 mg C L^{-1} Everglades F1 DOM) and near uniform pH, with salinity being the only major difference between treatment waters. Treatment waters of varying salinity (0.16−6.0 ppt) were prepared by mixing synthetic freshwater, designed to match the ionic background of average surface water in the Everglades,[46] and synthetic seawater prepared to 12.0 ppt salinity using "Sea-Salt" ASTM D 1141-98, Formula A (Lake Products Company LLC, Florissant, MO). DOM, previously purified by solid-phase extraction[53] and characterized for reduced S content[35] from porewater at Everglades Site F1 (3:1 mixture of the hydrophobic organic acid and transphilic organic acid DOM fractions, mimicking the natural distribution of the DOM in whole waters),[53] was added to each treatment water at a uniform concentration (final concentration = 5.5 mg C L^{-1}; Supporting Information Tables S2−S4). Across all salinity treatments, isotopically enriched $^{201}Hg(II)$ was pre-equilibrated with DOM for 24 h to establish strong Hg(II)−DOM aqueous complexes and resemble the speciation of aqueous Hg(II) in the native Everglades.[30] The DOM concentration was comparable to pristine marsh sites within Everglades National Park[23] and the molar concentration of strong thiol binding sites of DOM was estimated to exceed the $^{201}Hg(II)$ concentration >4-fold,[30] ensuring that the amended $^{201}Hg(II)$ was provided in a bioavailable and environmentally relevant aqueous species. Peat cores (n = 80, 16 × 5) were

https://doi.org/10.1021/acsearthspacechem.4c00124
ACS Earth Space Chem. XXXX, XXX, XXX−XXX

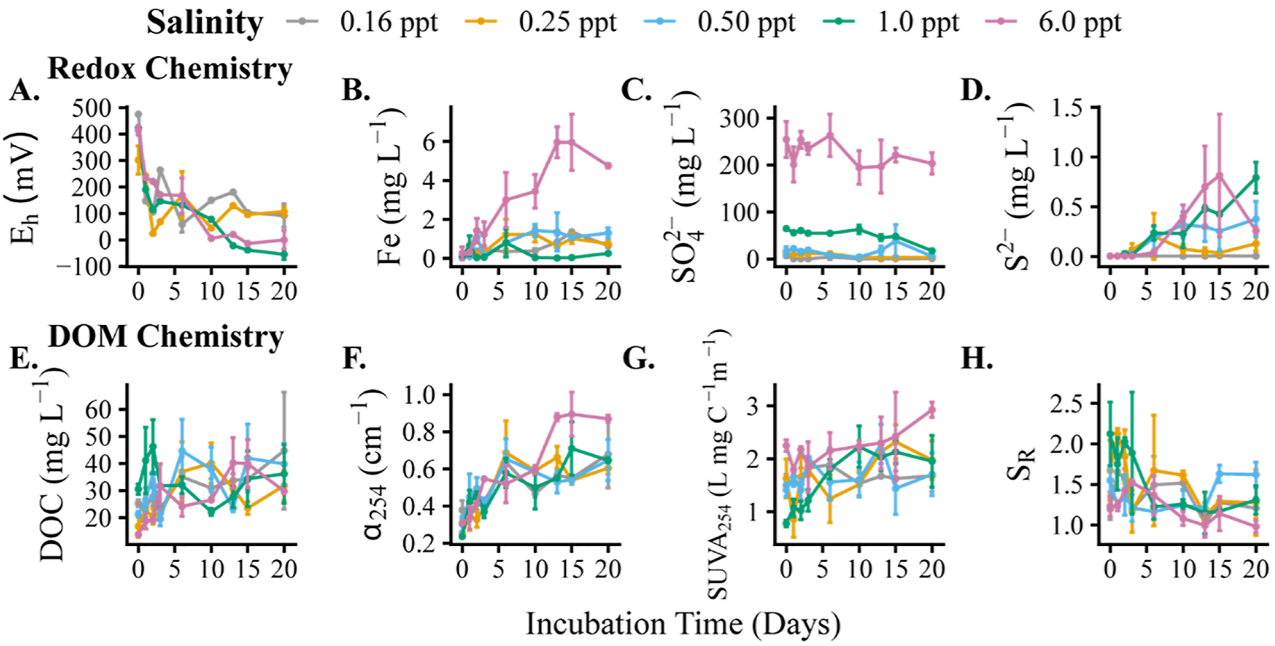

Figure 1. Porewater (A) redox potential (E_h) values at 6 cm depth from water surface compared to standard hydrogen electrode and porewater concentrations of (B) total iron (Fe), (C) sulfate (SO_4^{2-}), (D) total sulfide (S^{2-}), and (E) DOC concentration, (F) DOM decadic absorbance at 254 nm (α_{254}), (G) DOM specific ultraviolet absorbance at 254 nm ($SUVA_{254}$), and (H) DOM spectral slope ratio (S_R). In panel A, data points with no error bars represent values of a single replicate ($n = 1$) and data points with error bars represent the average values of experimental replicates ($n = 2$) and error bars represent the average deviation from the mean. ORP measurements for the 0.50 ppt treatment are not reported. In panels B–H, data points at time points t = 1, 2, 3, 10, 13, and 15 and 0, 6, and 20 days present average values of experimental duplicates (n = 2) and triplicates (n = 3), respectively, and error bars represent the average deviation from the mean. Outlier values in DOC concentration were removed ($n \leq 1$ per salinity treatment above 80 mg C L^{-1}) for clarity.

flooded with each of the equilibrated treatment waters (see Supporting Information Figures S3, S4 and Section S1.3). Additional cores at each salinity (n = 25, 5 × 5) were used to track biogeochemical changes in DOM chemistry at finer temporal resolution with no ^{201}Hg(II) amendment. Once filled with porewater, peat cores were covered with Parafilm (with holes to allow for gas exchange), wrapped in foil to prevent photochemical degradation of Hg species, and stored static on a laboratory bench at 25 ± 2 °C for the duration of the incubation.

Duplicate cores were sacrificially sampled after 1, 2, 3, 10, 13, and 15 days, and triplicate cores were sacrificially sampled after 0, 6, and 20 days. Profiles of dissolved $O_{2(g)}$ and redox potential (E_h) were measured on one of the duplicate cores, or two of the triplicate cores, for each treatment and time point, using a vertical profiler and microsensors that are nondestructive, to a depth of 6 cm into the peat (Supporting Information Figure S5). Next, porewater was collected from duplicate and triplicate cores by gently compressing the peat, filtered (0.45 μm), and subsampled for measurement of total sulfide (S^{2-}), pH, DOC concentration, DOM decadic absorbance at 254 nm (α_{254}) and spectral slope ratio (S_R, eqs S1 and S2),[54,55] total iron, inorganic anions (SO_4^{2-}, Cl^-, NO_3^-), total Hg, and MeHg; details on all measurements are provided in Supporting Information Section S1.4. The $SUVA_{254}$ (L mg C^{-1} m^{-1})[37] of DOM was calculated by dividing α_{254} (m^{-1}) by the DOC concentration (mg C L^{-1}). Peat samples collected from incubations were immediately frozen and then freeze-dried, and subsequently analyzed for total Hg and MeHg content. Distribution coefficients (K_d) were determined for ^{201}Hg(II) and Me^{201}Hg (K_d ^{201}Hg(II) and K_d Me^{201}Hg, respectively; eqs S3 and S4). All data collected from incubations are provided in the Supporting Information in an Excel workbook (*xlsx file format) and as an associated data release product.[56]

Thermodynamic Hg speciation calculations of porewaters was performed in MINEQL+ 5.0 to assess the (1) influence of ionic strength on Fe(II)-sulfide mineral solubility,[57−60] (2) Hg(II) speciation in porewaters in the presence of DOM and varying levels of sulfide and Cl^-,[57,61,62] and (3) aqueous speciation of MeHg in the presence of DOM and varying levels of Cl^- (specific conditions tabulated in Supporting Information Tables S5–S7).[63]

RESULTS AND DISCUSSION

Porewater Chemistry of Peat Incubations. For each of the five treatment salinities (0.16, 0.25, 0.5, 1.0, and 6.0 ppt), porewater pH fluctuated between 6 and 7 from day 0 to day 20 (Supporting Information Figure S6A) with no statistical difference between time at each salinity (p > 0.05, one-way ANOVA, n = 105) and an observed statistical effect of salinity on pH with higher salinity treatments exhibiting modestly lower pH values (p < 0.05, one-way ANOVA, n = 105). The observed circumneutral pH values of porewaters corresponded with other measurements of Everglades porewater at modest salinity of 3.5 ppt (pH = 6.8),[50] as well as field measurements of freshwater Everglades wetlands,[46] owing partly to the high buffering capacity of the carbonate Floridan aquifer platform that underlies the Everglades peat.[46] Porewater conductivity and chloride (Cl^-) concentrations (Supporting Information Figure S6B,C) of each salinity treatment were uniform through time, which confirmed that evaporative loss during the 20 day incubation was minimal.

The porewater chemistry data from peat incubations exhibited consistent trends of more reducing conditions with

https://doi.org/10.1021/acsearthspacechem.4c00124
ACS Earth Space Chem. XXXX, XXX, XXX−XXX

increased incubation time and notable differences in redox conditions between the five salinities. Peat cores were incubated with water saturated with dissolved $O_{2(g)}$, and all incubation porewaters were completely anoxic by day 1 ($O_{2(g)}$ < 0.01 mg L^{-1}) (see Supporting Information xlsx file). Porewater E_h, measured at 6 cm depth in the cores using the redox profiler (Supporting Information Figure S5), averaged 389 ± 32.3 mV (mean ± standard error, n = 6) across all salinities at day 0 and decreased as the experiment progressed (Figure 1A). Between 10 and 20 days, the 2 highest salinity treatments (1.0 and 6.0 ppt) demonstrated statistically lower E_h values (−54.4 ± 18.9 and 0.00 ± 35.0 mV at day 20, respectively; mean ± average deviation, n = 2) compared to the lowest two salinity treatments (0.16 ppt: 92.1 ± 43.8 mV, and 0.25 ppt: 107 ± 16.8 mV at day 20; mean ± average deviation, n = 2) (Tukey, p < 0.05, n = 20).

Concentration trends in total iron (Fe) within porewater varied with incubation time across the five salinity treatments (Figure 1B). The total Fe concentration was below the limit of detection in treatment waters used at the initiation of the experiment to saturate the peat cores (<0.01 mg L^{-1}) and <0.3 mg L^{-1} in porewaters for all salinities treatments at day 0. We observed an increase in total Fe concentration over the course of the incubation time frame with the highest concentrations measured in the 6.0 ppt treatment (e.g., 5.96 mg L^{-1} by day 13). By day 20, the 6.0 ppt treatment demonstrated the highest levels of porewater total Fe (4.8 ± 0.1 mg L^{-1}) (mean ± standard error, n = 3) and the 1.0 ppt treatment demonstrated the lowest Fe concentration (0.26 ± 0.05 mg L^{-1}) (mean ± standard error, n = 3), while the other treatments exhibited comparable and intermediate total Fe concentrations between the 1.0 and 6.0 ppt treatments. In the 0.25, 0.50, and 6.0 ppt treatments, there were significant correlations between porewater total Fe and DOC concentrations (Spearman's correlation, p < 0.05; Supporting Information Figure S7), whereas under 0.16 and 1.0 ppt treatments, these parameters were not significantly correlated (Spearman's correlation, p > 0.05).

Dissimilatory SO_4^{2-} reduction was evident at the four highest salinity treatments (0.25−6.0 ppt). Initial SO_4^{2-} concentrations of the porewaters were primarily reflective of the SO_4^{2-} concentrations in the treatment waters (Supporting Information Table S4) and established the hierarchy in SO_4^{2-} levels in porewaters at t = 0 days, which spanned from 7.0 ± 3.1 to 254 ± 29 mg L^{-1} (mean ± standard error, n = 3) in 0.16 and 6.0 ppt salinity treatments, respectively (Figure 1C). Cores flooded with 0.16 ppt treatment water, which contained 0.3 mg L^{-1} SO_4^{2-}, exhibited higher SO_4^{2-} concentrations in the porewater at t = 0 days (7.0 ± 3.1 mg L^{-1}) (mean ± standard error, n = 3) that also exceeded field conditions at this site during core collection (Supporting Information Table S1). We attribute this to the oxidation of organic S from the peat[64] during the flushing of cores with oxic treatment water, as the WCA-3A wetland where cores were collected likely experienced prior anthropogenic SO_4^{2-} inputs.[11,45] Sulfate applications enrich peat in organic S[65] that is susceptible to oxidation and release of SO_4^{2-}.[66] In general, porewater SO_4^{2-} concentration decreased over time across the five salinity treatments (Figure 1C). In the four treatments of 0.16−1.0 ppt salinity, 66−87% of initial SO_4^{2-} was depleted at day 20, whereas only 20% of the initial SO_4^{2-} was depleted in the 6.0 ppt treatment at day 20. Porewater total inorganic sulfide concentrations (measured as S^{2-} and representing the summation of $H_2S_{(aq)}$ and HS^- under the range of experimental pH) from both the 1.0 and 6.0 ppt treatments were significantly elevated (e.g., 0.79 ± 0.13 and 0.26 ± 0.03 mg L^{-1} at day 20, respectively; mean ± standard error, n = 3) compared to the freshwater 0.16 ppt treatment (<detection limit at all time points, n = 21) (p = 0.007 and p = 0.012 for 1.0 and 6.0 ppt, respectively; Dunnett, n = 105; Figure 1D). The 0.25 and 0.5 ppt salinity treatments showed decreasing SO_4^{2-} concentrations and subsequent increasing total sulfide concentrations with increased incubation time, which were only modestly higher than the 0.16 ppt treatment. Importantly, the measured total sulfide concentration across the 20 day incubation could only explain ≤1.5, 5, and 10% of the decrease of porewater SO_4^{2-} concentrations in the 6.0, 1.0, and 0.5 ppt treatments, respectively, which we attribute to sulfide removal processes discussed below.

DOC quantity and quality in the porewaters were highly variable within and across salinity treatments. Incubation peat cores were filled with treatment water containing 5.5 mg C L^{-1} Everglades F1 DOM. In comparison, day 0 porewater samples across the five treatments exhibited higher DOC concentrations (11.9−33.4 mg C L^{-1}) than the treatment waters (Figure 1E). Measurements of porewater DOC concentration at each treatment through time varied an order of magnitude (10−165 mg C L^{-1}) and did not exhibit consistent trends with increased incubation time across the five salinity treatments. Although the DOC concentrations were elevated and exceeded that of the typical observed porewater DOC concentration at WCA site 3A-H (17−23 mg C L^{-1}),[46] these elevated DOC concentrations are not atypical of porewaters from other nutrient-enriched sites in the Florida Everglades[35,46] and other SO_4^{2-}-rich peatlands.[67] Furthermore, DOC concentrations were highly variable both within salinity treatments and between replicate cores for specific time points, interpreted to reflect heterogeneity in the peat cores and the highly dynamic nature of organic C in the incubations. Previous incubation[68] and field studies[48] of sea level rise in the Florida Everglades demonstrated that increasing porewater DOC coincided with declines in soil bulk density as a function of increasing salinity, the latter attributed to increased organic C mineralization to CO_2.[48] In other coastal wetlands soils, simulated sea level rise (at ∼5−10 ppt) increased organic C mineralization rates due to increased availability of seawater SO_4^{2-} as a terminal electron acceptor,[49,68−70] with dissimilatory SO_4^{2-} reduction accounting for >95% of the organic C mineralization.[70] We can discount a major effect of DOC flocculation[71] at higher cation concentrations up to 6.0 ppt, as higher salinity treatments did not exhibit statistically lower DOC concentrations than lower salinity treatments. Thus, we interpret the observed changes in DOC concentration measured in our cores to reflect the cumulative effects of DOC removal by increased mineralization rates and DOC production through organic peat decomposition.[71]

In contrast to trends in DOC concentration, the composition of porewater DOM in peat incubations, measured as DOM $SUVA_{254}$ and S_R, exhibited discernible trends over the course of the incubations. The treatment water that was infused into cores had a DOM $SUVA_{254}$ value of 4.24 L mg C^{-1} m^{-1}, α_{254} value of 0.23 cm^{-1}, and spectral slope ratio (S_R) of 0.86, whereas porewaters at day 0 exhibited a lower DOM $SUVA_{254}$ (0.69−2.41 L mg C^{-1} m^{-1}), higher α_{254} (0.23−0.45 cm^{-1}) and higher S_R values (1.01−2.71) (Figure 1F−H). We interpret these early experimental changes in DOC character to have resulted from displacement and mobilization of small, nonaromatic DOM into porewaters due to initial filling of the cores with the experimental fluids.[37,55] The α_{254}, a measurement influenced by both DOC

https://doi.org/10.1021/acsearthspacechem.4c00124
ACS Earth Space Chem. XXXX, XXX, XXX−XXX

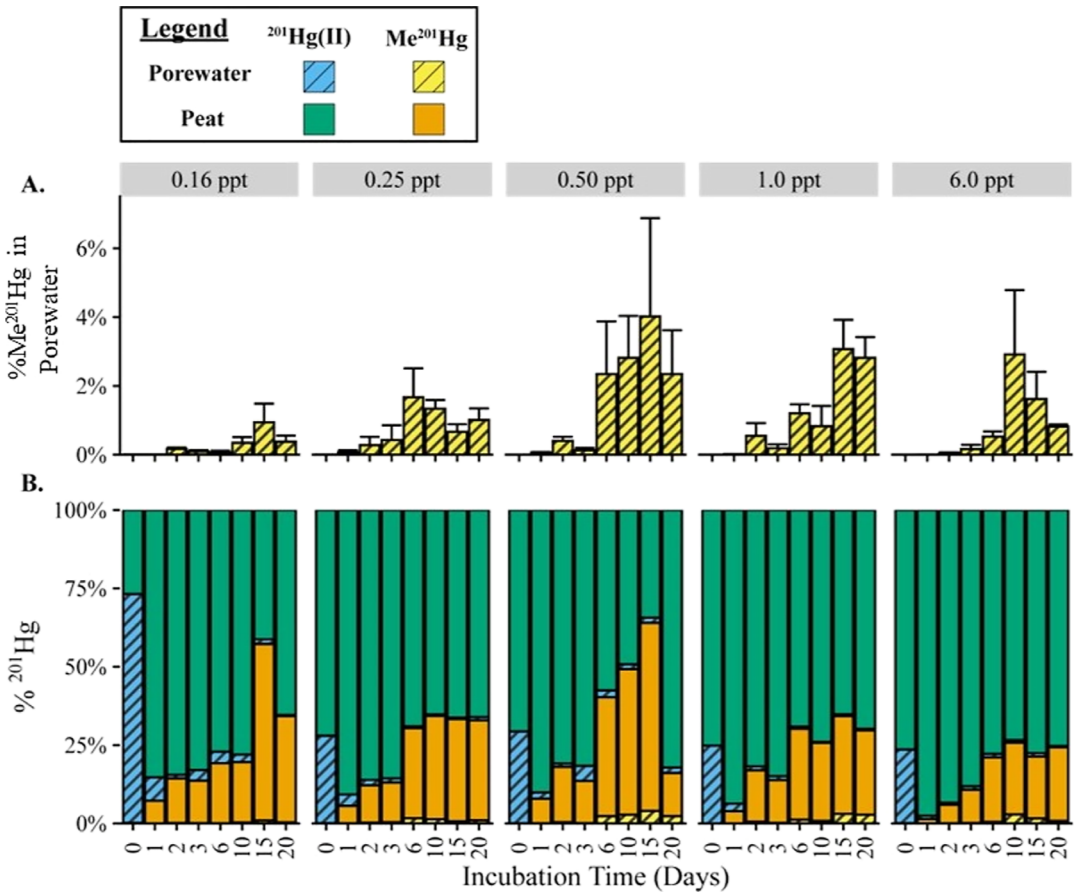

Figure 2. (A) Percentage of total ^{201}Hg as porewater Me^{201}Hg relative to the entire ^{201}Hg pool and (B) percentage of all Hg species relative to the entire ^{201}Hg pool (porewater and peat) vs incubation time from peat core experiments. Hashed bars represent porewater ^{201}Hg species and solid bars represent peat ^{201}Hg species. Yellow and orange bars represent Me^{201}Hg and green and blue bars represent ^{201}Hg(II). Data points present average values of experimental replicates (n = 2) and error bars represent the average deviation from the mean.

concentration and DOM aromaticity, shows consistent monotonic increases through time across all salinity treatments (Figure 1F), with the 6.0 ppt treatment demonstrating statistically higher mean α_{254} than all other salinity treatments from day 10 onward (Tukey, $p < 0.05$, $n = 35$). DOM SUVA$_{254}$ measurements generally increased with incubation time for each treatment, indicating increasing aromaticity of the DOM pool through time (Figure 1G).[37] This trend was most evident in the 1.0 ppt treatment, where the DOM SUVA$_{254}$ increased from 0.78 ± 0.05 to 2.0 ± 0.4 L mg C^{-1} m^{-1} (mean $\pm$ standard error, n = 3) from day 0 to day 20. In the 6.0 ppt salinity treatment, the DOM SUVA$_{254}$ values were elevated throughout the 20 day experiment compared to other salinity treatments and were statistically different from the freshwater 0.16 ppt treatment ($p <$ 0.001, Dunnett, n = 105). Further, S_R, an optical metric that scales negatively with DOM molecular weight,[55] showed a consistent monotonic decrease with increased incubation time across treatment salinities (Figure 1H). This was most evident in the 0.25, 1.0, and 6.0 ppt treatments, indicating that the DOM pool increased in molecular weight with increased incubation time. Importantly, low molecular weight organic acids, which do not absorb in the UV−vis of our measured range of wavelengths, can exhibit unique dynamics in soil flooding microcosms[72,73] but were not measured and could have influenced trends in DOC concentration (and thus SUVA$_{254}$ values). Yet, taken together, trends in DOM optical indices suggest that, compared to the low salinity treatment (0.16 ppt), the DOM pool in the four higher salinity amendments becomes more enriched in higher molecular weight molecules through time as aromatic DOM molecules were mobilized from the peat and low molecular-weight and aliphatic DOM molecules were preferentially mineralized in porewaters.

We interpret that these biogeochemical dynamics (filter-passing total Fe, SO_4^{2-}, total sulfide, and DOC concentration and DOM composition) in porewaters were driven by microbial processes and potential iron sulfide (FeS), DOM, and peat interactions. The observed rapid decreases in SO_4^{2-} concentration and E_h concomitant with increases in sulfide concentration across the incubations demonstrate that the microbial communities in the peat cores quickly deplete dissolved $O_{2(g)}$ and switch to dissimilatory SO_4^{2-} reduction to drive anaerobic respiration. Sulfate reduction was likely responsible for the observed increase in high molecular weight DOM due to increased peat degradation by SO_4^{2-} reducing bacteria,[28,29,35] and the overall shift in DOM composition toward more aromatic molecules is consistent with microbial processing.[72,74] The sulfur mass balance analysis, which showed that the majority of SO_4^{2-} reduced was not present as total sulfide, is likely due to a combination of sulfide removal processes including the sulfurization of peat[64,65] and DOM,[35,67] $H_2S_{(g)}$ evasion, and $FeS_{(s)}$ precipitation. We interpret the concentration dynamics of porewater total Fe to be linked to the net effect of the comobilization of Fe(II) from peat with DOM (Supporting Information Figure S7) and reassociation of Fe(II) with peat via

https://doi.org/10.1021/acsearthspacechem.4c00124
ACS Earth Space Chem. XXXX, XXX, XXX−XXX

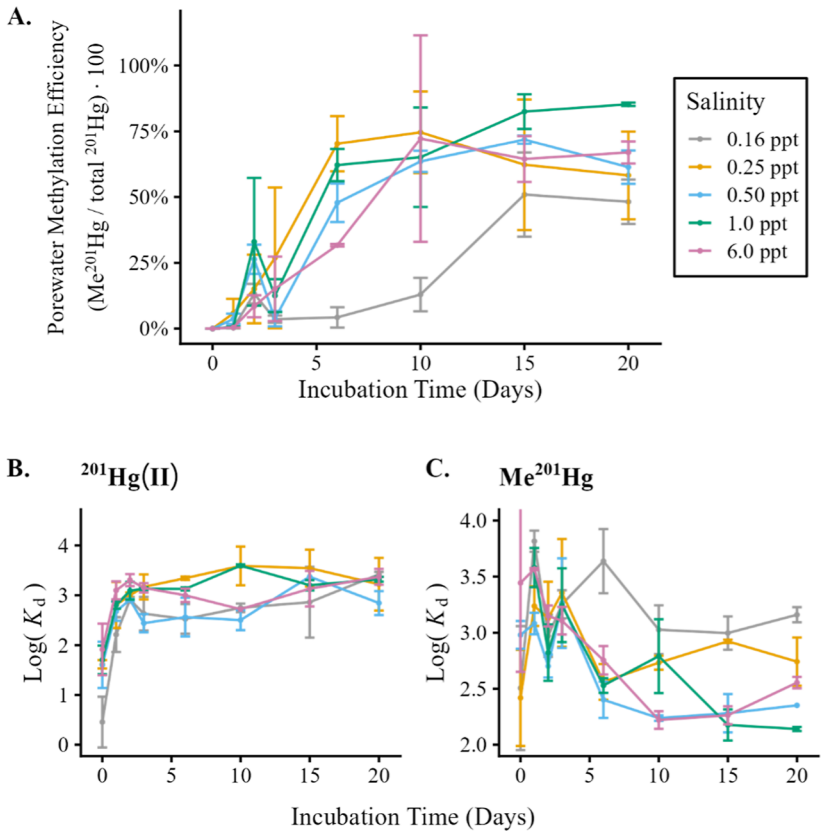

Figure 3. (A.) Porewater methylation efficiency presented as the percent of total porewater ^{201}Hg as Me^{201}Hg and distribution coefficients (log(K_d); L kg^{-1}) of (B) ^{201}Hg(II) and (C) Me^{201}Hg as a function of incubation time. Data points present average values of experimental replicates (n = 2) and error bars represent the average deviation from the mean.

the formation of $FeS_{(s)}$, the latter linked to the activity of SO_4^{2-} reducing bacteria. The removal of Fe(II) through $FeS_{(s)}$ formation would be influenced by the rate of SO_4^{2-} reduction, which could explain why porewater total Fe was low in the 1.0 ppt salinity at high sulfide (Figure 1D) yet higher and correlated to DOC concentration at both lower (0.5 ppt) and higher salinity (6.0 ppt) (Supporting Information Figure S7). However, we cannot discount the possibility of Fe(II) release via microbial reductive dissolution of Fe(III) oxyhydroxides. DOM likely stabilized Fe(II) via aqueous complex formation.[75] Further, thermodynamic speciation calculations confirms a negligible impact of ionic strength on Fe solubility from $FeS_{(s)}$ (Supporting Information Figure S8). Thus, we attribute differences between the five salinities in total Fe release dynamics to varying levels of SO_4^{2-} reduction and DOC release dynamics. In summary, higher salinity water, which had higher SO_4^{2-} concentration, stimulated the metabolism of SO_4^{2-} reducing bacteria leading to elevated concentrations of sulfide and Fe, lower E_h, and the accumulation of more aromatic DOM in porewater.

Mercury Methylation in Peat Incubations. The mass of total ^{201}Hg in each core was determined for each treatment salinity and each time point (Supporting Information Figure S9). On average, cores received 302 ± 30 ng ^{201}Hg(II) (mean ± standard error, n = 80) at the start of the experiment and were not statistically different between the five salinities (one-way ANOVA, $p > 0.1$, $n = 80$); the added ^{201}Hg(II) represented 4.1 ± 3.4% (mean ± standard error, n = 80) of total ambient Hg. However, the total amount of ^{201}Hg(II) tracer added to each core was variable due to how the cores were filled. Within each salinity treatment, cores that were filled first received higher total ^{201}Hg(II) levels, while cores that were filled last received lower total ^{201}Hg(II) levels. We hypothesize this is due to the peat scavenging of aqueous ^{201}Hg(II), likely as Hg(II)-thiol complexes,[76] while the cores were being flushed with the reservoir of treatment water. In Supporting Information Section S2 we discuss how the differences in mass ^{201}Hg(II) had minimal effect on the study interpretations. Accordingly, to account for differences in the ^{201}Hg(II) tracer added to each core, ^{201}Hg(II) methylation results are relativized to the total ^{201}Hg tracer within each core.

The influence of salinity on ^{201}Hg(II) methylation in core incubation experiments was evaluated in porewater and peat. Figure 2 presents the abundance of porewater and peat ^{201}Hg, as Me^{201}Hg and ^{201}Hg(II), as a percentage of the total ^{201}Hg tracer over the 20 day incubation (concentration results are presented in Supporting Information Figure S10). From day 0 to day 1, porewater ^{201}Hg(II) concentrations dramatically declined in each of the five salinity treatments, concurrent with increases in peat ^{201}Hg(II) concentration; these results indicate rapid but incomplete partitioning of the ^{201}Hg(II) tracer to the peat within the first day of the experiment. Me^{201}Hg in the peat and porewater was near or below the detection limit at t = 0 days, as the treatment water contained exclusively ^{201}Hg(II). At day 1, Me^{201}Hg production was detectable and variable across the five treatments (net methylation rate over 1 day = 1.4−7.9%), which is comparable to the reported range of Hg(II) methylation observed in Everglades peat soils (typically 1−8% over 24 h).[6,10,66] Notably, at day 1, Me^{201}Hg production was higher in the three lower salinity treatments (0.16, 0.25, and 0.5 ppt) compared to the two higher salinity treatments (1.0 and 6.0

https://doi.org/10.1021/acsearthspacechem.4c00124
ACS Earth Space Chem. XXXX, XXX, XXX−XXX

ppt), suggesting a faster response to MeHg formation at the early onset of saltwater intrusion. The 0.16 and 0.5 ppt treatments reached maximum levels of methylation across all treatments, with total methylation of 49−64% at 10−15 days in the 0.5 ppt treatment and 57% at day 15 in the 0.16 ppt treatment. The 6.0 ppt treatment demonstrated the lowest $Me^{201}Hg$ production by day 15, with a mean total methylation percentage of 21%.

Importantly, notable differences were observed in the timing and magnitude of $Me^{201}Hg$ production and accumulation in porewaters. In each of the elevated salinity treatments (0.25−6.0 ppt), a greater proportion of newly formed $Me^{201}Hg$ was observed to accumulate in porewaters relative to the 0.16 ppt treatment, as indicated by yellow hashed bars in Figure 2 (and $Me^{201}Hg$ concentration in Supporting Information Figure S10A). The mean fraction of total ^{201}Hg as porewater $Me^{201}Hg$ in the 0.16 ppt treatment was low in the first 6 days (≤0.17%), eventually reaching a maximum of 0.94% on day 15. Conversely, in the 1.0 ppt treatment, the fraction of total ^{201}Hg as porewater $Me^{201}Hg$ increased to 0.55% by day 2 and 3.1% by day 15. Similar results were observed for the 6.0 ppt treatment, with the fraction of total ^{201}Hg as porewater $Me^{201}Hg$ increased to 0.53% on day 6, and reached a maximum of 2.9% on day 10.

The net efficiency of $^{201}Hg(II)$ methylation and/or accumulation in the porewater (described hereafter as "methylation efficiency") was determined by quantifying the percentage of total porewater ^{201}Hg tracer converted to porewater $Me^{201}Hg$ at each time point (Figure 3A). Because the experiment design did not permit us to account for the demethylation of $Me^{201}Hg$ to $^{201}Hg(II)$,[77] the observations solely reflect net methylation efficiency at each time point. For the 0.16 ppt treatment, the methylation efficiency was low from 0 to 10 days, increased from 10 to 15 days, and plateaued to a maximum of 50 ± 7.4% (mean ± standard error, $n = 4$) between 15 and 20 days. In contrast, the 0.25, 0.5, 1.0, and 6.0 ppt treatments exhibited methylation efficiencies that increased dramatically from days 0−10 and plateaued from days 10−20 between 72 and 85%. At time points beyond 3 days, each elevated salinity treatment (0.25−6.0 ppt) had statistically higher methylation efficiency compared to the 0.16 ppt freshwater treatment (Dunnett, $p < 0.05$, $n = 40$) but did not differ significantly from one another (Tukey, $p > 0.05$, $n = 40$). Taken together, these results demonstrate that the accumulation of new $Me^{201}Hg$ in porewaters was higher at elevated salinity compared to the 0.16 ppt treatment, both at short time intervals (3−10 days) and at 20 days.

Distribution coefficients (K_d) of $^{201}Hg(II)$ and $Me^{201}Hg$ were quantified across each treatment through time (Figure 3B,C) to determine salinity effects on the partitioning of Hg species between peat and porewater. Across all salinity treatments, K_d values of $^{201}Hg(II)$ (Figure 3B) increase rapidly from day 0 onward (with no statistical differences observed between salinities), governed by the rapid binding of Hg(II) with peat likely via organic and inorganic reduced S.[76] For $Me^{201}Hg$ (Figure 3C), however, K_d values decreased with increased incubation time for each salinity, most drastically in the elevated salinity treatments of 0.5, 1.0, and 6.0 ppt. By day 15, each of those treatments reached mean $Me^{201}Hg$ log K_d values of 2.28 ± 0.17, 2.18 ± 0.14, and 2.26 ± 0.08 respectively, compared to 3.00 ± 0.19 and 2.92 ± 0.01 (mean ± average deviation, $n = 2$) for the 0.16 and 0.25 ppt treatments. By days 15 and 20, the 1.0 ppt treatment reached the lowest mean log K_d values of all treatments (2.18 ± 0.14 and 2.14 ± 0.02, respectively; mean ± average deviation, $n = 2$). Significant differences were observed in log K_d values at time points >3 days between the 0.16 ppt treatment and three elevated salinity treatments (0.5, 1.0, and 6.0 ppt; Dunnet, $p < 0.01$, $n = 40$). These results demonstrate that at elevated salinity, newly formed MeHg in inundated peat soil has a greater distribution in porewaters, with evidence of moderate saltwater intrusion of 0.5 ppt having the largest effect (Figure 3C).

We further evaluated the effect of salinity on Hg fate by evaluating if the ambient Hg pool in the peat and porewaters displayed increased Hg(II) methylation and accumulation of MeHg in porewaters in response to modest salinity increases (Supporting Information Figure S11). Consistent with the $^{201}Hg(II)$ spike (Figure 3), the ambient porewater % MeHg (1) was significantly elevated in the four highest salinity treatments compared to the 0.16 ppt treatment, (2) steadily increased with incubation time, and (3) was a substantial proportion of the ambient porewater total Hg (36−85% at day 20; Supporting Information Figure S11A). The distribution coefficient of ambient Hg(II) was uniform over the course of the experiment (Supporting Information Figure S11B), which was anticipated because the reservoir of peat Hg(II) is expected to primarily be unavailable to remobilization. For ambient MeHg, in contrast, the log K_d was ∼5.0 at the start of the incubations, which is similar to ambient conditions measured across Everglades wetlands,[78] and decreased to <3.0 with increased incubation time at the four higher salinities (Supporting Information Figure S11C). Thus, modest increases in salinity resulted in an increase in the formation and accumulation of ambient MeHg in porewaters. In summary, the methylation of ambient Hg(II) in the cores was highly consistent in magnitude, timing, and extent as the $^{201}Hg(II)$ spike over a 20 day incubation, providing clear evidence that the $^{201}Hg(II)$ tracer was representative of ambient Hg(II) and responsive to biogeochemical processes observations in cores over the 20 day incubation.

Biogeochemical Effects of Salinity Increases on Mercury Methylation in Peat Soils. This study presents the first detailed laboratory assessment of the response of Hg(II) methylation to moderate salinity increases in coastal peat soils. Our findings suggest that the inundation of peat by moderate salinity water, common at the onset of saltwater intrusion, results in rapid and enhanced MeHg accumulation in porewaters, as evidenced by distribution coefficients (K_d) and methylation efficiencies of the $^{201}Hg(II)$ tracer (Figure 3) and ambient Hg(II) (Supporting Information Figure S11). Although under the conditions of the experiment, a similar magnitude of net MeHg formation was observed in the peat across the five salinities over 20 days (Figure 2) the accumulation of MeHg in porewaters was strictly observed at higher salinities (≥0.25 ppt; SO_4^{2-} = 7.2 mg L^{-1}). Concomitant with overall MeHg production and porewater MeHg accumulation, we observed increases in porewater DOM α_{254} and $SUVA_{254}$ and decreases in DOM S_R (Figure 1F−H), indicating increases in the concentration of aromatic DOM with time during the 20 day incubations.[37,55] Further, at higher salinity treatments (0.25−6.0 ppt), MeHg production was observed concurrent with increases in porewater sulfide concentrations due to dissimilatory SO_4^{2-} reduction (Figure 1C,D). The biogeochemical processes governing the production and partitioning of MeHg in response to salinity increases, with an emphasis on aqueous ligands of $^{201}Hg(II)$ and MeHg (DOM, inorganic sulfide, Cl^-) and microbial processes, are evaluated below.

https://doi.org/10.1021/acsearthspacechem.4c00124
ACS Earth Space Chem. XXXX, XXX, XXX−XXX

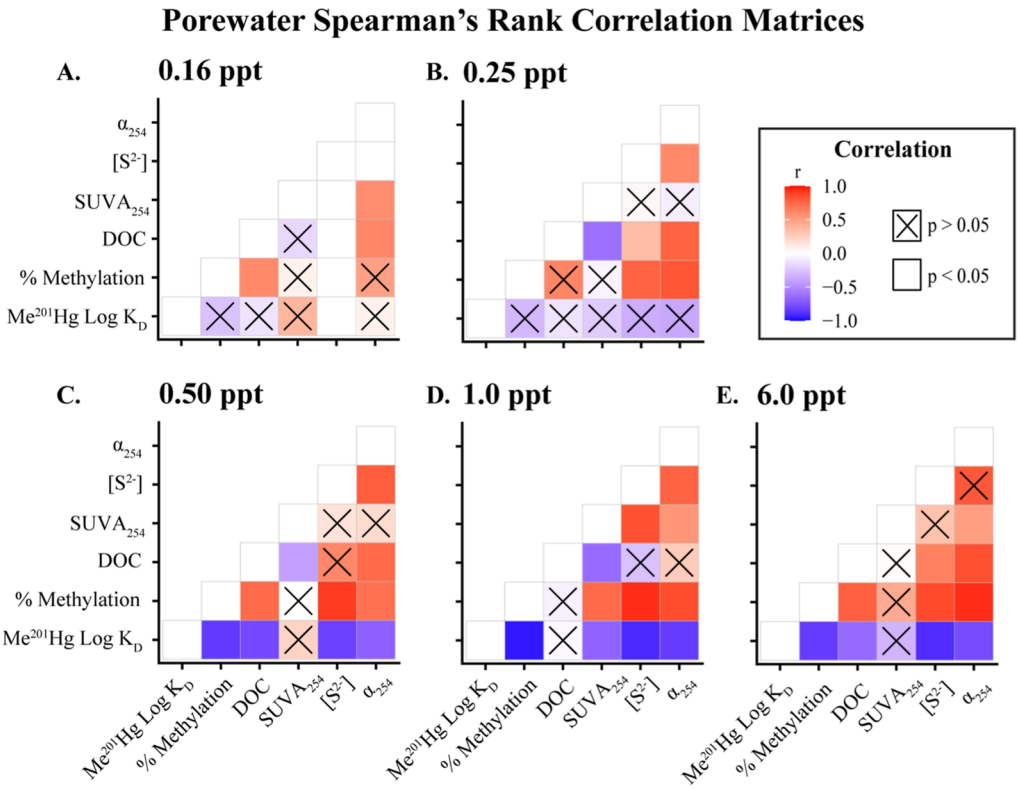

Figure 4. Spearman's rank correlation matrices for porewaters from treatment salinities (A) 0.16, (B) 0.25, (C) 0.50, (D) 1.0, and (E) 6.0 ppt. Darker red boxes at the intersection between two parameters indicate a stronger positive correlation; darker blue boxes represent a stronger negative correlation. Boxes at intersections between two significantly statistically correlated parameters (Spearman's rank, $p < 0.05$) are represented as an open box. Boxes at intersections between two insignificantly statistically correlated parameters (Spearman's rank, $p > 0.05$) are represented by a box with a black X symbol. S^{2-} concentration correlations are omitted from panel A due to S^{2-} being below the detection limit in all but one core at 0.16 ppt.

Linear regression and Spearman's rank correlation analyses between porewater methylation efficiency and pertinent parameters of geochemical ligands (total sulfide concentration, DOC concentration, DOM $SUVA_{254}$, and α_{254}) provide evidence of the underlying drivers of increasing formation and accumulation of MeHg in porewater in higher salinity treatments (Figure 4). First, at each elevated salinity treatment (0.25−6.0 ppt), there were strong positive correlations between sulfide concentrations and both porewater methylation efficiency (Spearman's rank, $p < 0.05$) and porewater $Me^{201}Hg$ concentrations (Spearman's rank, $p < 0.002$). The 1.0 ppt treatment displays the strongest positive trends between sulfide and MeHg and methylation efficiency (Figure 4D). Second, DOM concentration and composition were also controlling factors in influencing the lability of aqueous Hg(II) to methylation. Across all five salinities, the DOM α_{254}, which encompasses both DOC concentration and DOM aromaticity, correlated positively with porewater methylation efficiency. Speciation calculations of Hg(II) in porewaters (detailed in Section 1.5 of the Supporting Information, Figure S13) at experimental DOM and sulfide concentrations supports the predicted presence of β-$HgS_{(s)}$ under most conditions in this experiment (sulfide >0.03 mg L^{-1}). When sulfide was below the limit of detection (<5 μg L^{-1}), aqueous Hg(II)−DOM complexes were predicted to dominate Hg(II) speciation even in the presence of Cl^- at brackish concentrations.

DOM and SO_4^{2-} also had a significant impact on the distribution coefficient of $Me^{201}Hg$. The distribution coefficients of $Me^{201}Hg$ were significantly lower at higher salinity treatments, indicating a higher proportion of MeHg in porewater compared to peat. The Spearman's rank correlation analysis shows that, for salinity 0.50 to 6.0 ppt, the log K_d for $Me^{201}Hg$ was significantly negatively correlated with DOM α_{254} (Figures 4C−E and 5). We interpret this result to reflect the strong binding of MeHg to DOM in porewaters (stability constants for MeHg−DOM ranging from 10^{12} to $10^{16.5}$ via thiol groups);[63,79] salinity induced release and microbial processing of DOM in pore waters (Figure 1) increased the concentration of DOM to complex MeHg, as observed for both $Me^{201}Hg$ (Figures 3 and 5) and ambient MeHg (Supporting Information Figure S11). Aqueous Cl^-, an important aqueous ligand for MeHg in estuarine waters,[7] was at a higher concentration in elevated salinity treatments (Supporting Information Table S4). However, geochemical speciation calculations for MeHg in porewaters, conducted at an average DOC concentration of porewaters across the range of Cl^- of the five salinities, showed that ≥97.6% of the MeHg was present as MeHg−DOM complexes between 0.25 and 6.0 ppt (detailed in Section S1.5 and Figure S14 of the Supporting Information). Thus, we can discount the effect of Cl^- as an aqueous ligand influencing MeHg speciation and distribution coefficients up to 6.0 ppt salinity under the high DOC concentration here. Taken together, these observations support a conceptual understanding that that elevated SO_4^{2-} at higher salinities results in increased concentrations of aqueous ligands (DOM, sulfide) that enhance the production and stabilization of MeHg in porewaters.

Greater SO_4^{2-} concentrations due to elevated salinity also govern Hg biogeochemistry by influencing microbial processes linked to MeHg formation. Dissimilatory SO_4^{2-} reduction was evident based on the formation of sulfide as early as 2−3 days

https://doi.org/10.1021/acsearthspacechem.4c00124
ACS Earth Space Chem. XXXX, XXX, XXX−XXX

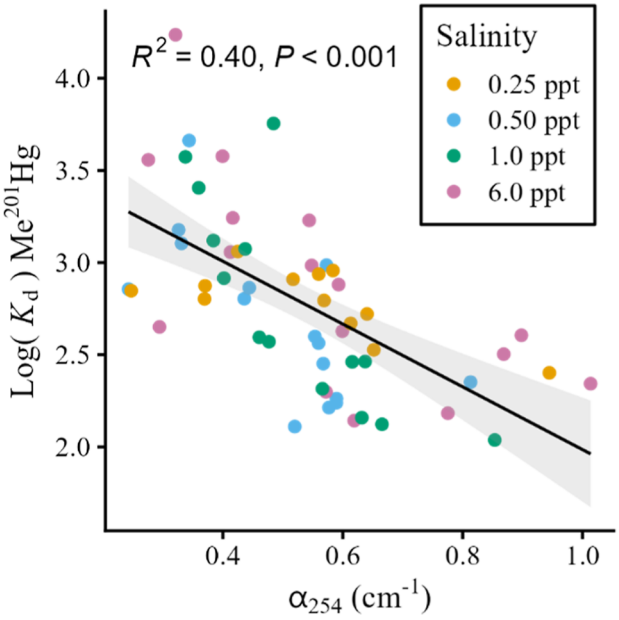

Figure 5. Linear correlation between the distribution coefficient of $Me^{201}Hg$ ($\log(K_d)$; L kg^{-1}) and the DOM absorbance at 254 nm (α_{254}, cm^{-1}) for the four highest salinity treatments. Statistical outliers for distribution coefficient of $Me^{201}Hg$ ($\log(K_d)$; L kg^{-1}) (n = 4 at 0.25 ppt) were identified and removed from the regression.

following inundation in 0.25−6.0 ppt treatments and, as noted above, sulfide concentration correlates to MeHg formation across a range of salinities. Experimental studies in the Everglades highlight the stimulation of MeHg production by SO_4^{2-}.[10,25] However, in freshwater portions of the Everglades that have similar SO_4^{2-} concentrations (from agricultural sources)[35,45,46] as the experimental conditions used in this study (0.20−454 mg L^{-1}), microorganisms with the dissimilatory SO_4^{2-} reduction genes (e.g., *dsrA*) did not possess the prerequisite genes for Hg(II) methylation (*hgcAB*).[6] In other freshwater aquatic environments with elevated SO_4^{2-}, microorganisms with the dissimilatory SO_4^{2-} reduction genes (*dsrA*) do possess the *hgcAB* gene pair.[80−82] This observation highlights the need for further research to better understand the exact role of SO_4^{2-} reducing microorganisms in MeHg production across a range of environmental conditions. SO_4^{2-} reducing bacteria may operate in syntrophy with methanogens to produce MeHg;[6,25,27] thus, it is unclear if SO_4^{2-} reducing bacteria are directly or indirectly involved in Hg(II) methylation in this system. While Fe reducing bacteria are also known to produce MeHg, there was no evidence of *hgcAB* in metagenomes of iron-reducing bacteria within freshwater environments of the Everglades[8] further suggesting that these organisms do not play an important role in MeHg production in this study. Ultimately, future microbial studies would fill a key knowledge gap on the importance of SO_4^{2-} reducing bacteria on MeHg formation in coastal environments experiencing sea level rise.

Together, these results highlight the complex influence of SO_4^{2-} on MeHg formation and partitioning. Dissimilatory SO_4^{2-} reduction indirectly influenced Hg(II) methylation by increasing Hg(II) bioavailability via the formation of nano-β-$HgS_{(s)}$, enhancing DOM sulfurization,[35] and/or increasing DOC concentration and aromaticity of DOM.[32,33] The stimulation of SO_4^{2-} reduction at elevated salinities is expected to increase the rates of anaerobic respiration and organic C mineralization of peat organic matter and DOM.[28,49,69,70,83] This increase in organic C mineralization is evident in both the 1.0 and 6.0 ppt treatments, where significant increases in DOM $SUVA_{254}$ (Figure 1G) and α_{254} (Figure 1F) were observed with increased incubation time. We interpret these observations to reflect a DOM pool becoming more aromatic at longer incubation times due to preferential microbial mineralization of lower molecular weight DOM and release of high molecular weight, aromatic DOM from peat. These processes are expected to enhance porewater Hg(II) concentrations (via complexation with DOM)[30] and bioavailability to methylating microbes, as has been shown in the field with complex microbial consortium[6] and the laboratory with pure cultured organisms.[33,34,36] Further, DOM released at higher salinities is expected to stabilize the produced MeHg in porewaters compared to low salinity, SO_4^{2-} free treatment. The multifaceted role of SO_4^{2-} on Hg biogeochemistry observed in our microcosm peat cores agrees with previous observations of the stimulation of Hg(II) methylation by SO_4^{2-} in the freshwater[6,10,11] and coastal Florida Everglades,[23] and other freshwater wetlands.[20−22] Further, the observed production and mobilization of MeHg from peat as a result of saltwater intrusion in this study aligns with field observations of the redistribution of MeHg between peat and porewater in responses to increases[38] and decreases[84] in SO_4^{2-} loading.

This study supports a conceptual model whereby the onset of saltwater intrusion could have profound impacts on the cycling of Hg in the Florida Everglades and other coastal peatlands on both short- and long-term time scales. Due to the gentle elevation gradient of the Shark River Slough and the southern Florida Everglades,[42] extensive areas of coastal wetlands can be inundated by wind- and storm-driven surges[18] and seasonal hydrologic fluctuations[17] attributed to the freshwater delivery to wetlands. These events will be exacerbated by rising sea levels due to climate change.[17] Our work further suggests that even a brief influx of seawater SO_4^{2-} from storm events or tidal cycles to freshwater peat with as little as 0.25 ppt (~10 s mg L^{-1} SO_4^{2-}) could exacerbate net methylation of Hg(II) in porewaters, as these conditions are observed as ideal for maximum MeHg production in many environments with intermediate levels of sulfide.[10,85] Under tidal conditions, produced MeHg that is complexed to DOM and stabilized in porewaters (i.e., lower log K_d values) (Figures 3C and 5) is available to be transported to coastal waters through tidal pumping, a phenomenon observed in coastal Everglades sites with MeHg mobilized with high aromatic DOM.[9] Storm surges can often result in the ponding of high salinity waters far inland,[18] and may have a similar effect. Further, as these ponded conditions recede, the draining waters would carry with them elevated levels of mobilized MeHg. Our findings further suggest that MeHg formation rate in response to SO_4^{2-} inputs may be slower at higher salinities compared to lower salinities, as the accumulation of MeHg and sulfide in porewater was demonstrably slower at 6.0 ppt than at lower salinities (0.25−1.0 ppt) (Figures 1D and 2). The underlying reasons for this observation require more investigation but may be due to osmotic stress on microbial communities at higher salinities.[86] Our results contrast an evaluation of coastal wetlands at three salinities in South Carolina (<0.30, <5.0, and 2−10 ppt), which reports lower ambient MeHg concentration at higher salinities up to 10 ppt in wetlands that had undergone transformations due to prolonged salinity increases.[87] This discrepancy may reflect the long-term versus short-term MeHg response to sea level rise, with the former resulting in wetland

https://doi.org/10.1021/acsearthspacechem.4c00124
ACS Earth Space Chem. XXXX, XXX, XXX−XXX

transformations that decrease organic C stocks in soils[83] over a time frame greater than those evaluated in this study.

The implications of elevated rates of MeHg production due to salinity increases may enhance MeHg export[9] and uptake in the aquatic food web.[13,15,44] This may explain why a survey of game fish from coastal Everglades National Park observed the highest concentrations of MeHg at the intersection of marine and freshwaters,[15] which could have implications for humans[5] and marine mammals.[44] Coastal communities historically have the highest exposure of MeHg through consumption of fish and shell-fish,[5] which could be exacerbated by biogeochemical changes to coastal wetlands as a result of sea level rise. Future field-based research would aid in filling key knowledge gaps on the linkages between saltwater intrusion and the biogeochemistry of MeHg formation in coastal wetlands vulnerable to sea level rise[16] under different hydrologic regimes (e.g., tidal cycles, storm surges, or changes in seasonal freshwater delivery), ecological impacts to coastal environments (e.g., mangrove dieback), and consequent changes in the DOM pool, peat integrity, and microbial community governing MeHg formation.

■ ASSOCIATED CONTENT

Supporting Information

The Supporting Information is available free of charge at https://pubs.acs.org/doi/10.1021/acsearthspacechem.4c00124.

Supporting Information on peat core collection (S1.1), porewater chemistry (S1.2), incubations (S1.3), water and peat analyses (S1.4), thermodynamic speciation calculations (S1.5), supporting interpretations (S2), and supporting figures and tables (S3) (PDF)

All data from incubations are provided in an xlsx file (XLSX)

■ AUTHOR INFORMATION

Corresponding Author

Brett A. Poulin − *Department of Environmental Toxicology, University of California Davis, Davis, California 95616, United States;* orcid.org/0000-0002-5555-7733; Phone: +1 530 754 2454; Email: bapoulin@ucdavis.edu

Authors

Bryce A. Cook − *Department of Environmental Toxicology, University of California Davis, Davis, California 95616, United States*

Benjamin D. Peterson − *Department of Environmental Toxicology, University of California Davis, Davis, California 95616, United States;* orcid.org/0000-0001-5290-9142

Jacob M. Ogorek − *U.S. Geological Survey Mercury Research Laboratory, Madison, Wisconsin 53726, United States*

Sarah E. Janssen − *U.S. Geological Survey Mercury Research Laboratory, Madison, Wisconsin 53726, United States;* orcid.org/0000-0003-4432-3154

Complete contact information is available at: https://pubs.acs.org/10.1021/acsearthspacechem.4c00124

Notes

The authors declare no competing financial interest.

■ ACKNOWLEDGMENTS

Support was provided by the U.S. Geological Survey Greater Everglades Priority Ecosystems Science (GEPES) Program, a grant from The Everglades Foundation and VoLo Foundation, and the UC Davis Agricultural Experiment Station (AES). We thank three anonymous reviewers and D. P. Krabbenhoft (USGS) for providing constructive suggestions that improved the study. Any use of trade, firm, or product names is for descriptive purposes only and does not imply endorsement by the U.S. Government.

■ REFERENCES

(1) UN Environment. *Global Mercury Assessment 2018*; UN Environment Programme, Chemicals and Health Branch Geneva: Switzerland, 2019.

(2) Hsu-Kim, H.; Kucharzyk, K. H.; Zhang, T.; Deshusses, M. A. Mechanisms Regulating Mercury Bioavailability for Methylating Microorganisms in the Aquatic Environment: A Critical Review. *Environ. Sci. Technol.* **2013**, *47*, 2441−2456.

(3) Bravo, A. G.; Cosio, C. Biotic Formation of Methylmercury: A Bio-Physico-Chemical Conundrum. *Limnol. Oceanogr.* **2020**, *65*, 1010−1027.

(4) Wiener, J. G.; Krabbenhoft, D. P.; Heinz, G. H.; Scheuhammer, A. M. Ecotoxicology of Mercury. In *Handbook of Ecotoxicology*, 2nd ed.; Hoffman, D. J., Rattner, B. A., Burton, G. A., Cairns, J. C., Eds.; Lewis Publishers: Boca Raton, FL, 2003; pp 409−463.

(5) Mahaffey, K. R.; Clickner, R. P.; Jeffries, R. A. Adult Women's Blood Mercury Concentrations Vary Regionally in the United States: Association with Patterns of Fish Consumption (NHANES 1999−2004). *Environ. Health Perspect.* **2009**, *117*, 47−53.

(6) Peterson, B. D.; Krabbenhoft, D. P.; McMahon, K. D.; Ogorek, J. M.; Tate, M. T.; Orem, W. H.; Poulin, B. A. Environmental Formation of Methylmercury Is Controlled by Synergy of Inorganic Mercury Bioavailability and Microbial Mercury-methylation Capacity. *Environ. Microbiol.* **2023**, *25*, 1409−1423.

(7) Black, F. J.; Poulin, B. A.; Flegal, A. R. Factors Controlling the Abiotic Photo-Degradation of Monomethylmercury in Surface Waters. *Geochim. Cosmochim. Acta* **2012**, *84*, 492−507.

(8) Blanchfield, P. J.; Rudd, J. W. M.; Hrenchuk, L. E.; Amyot, M.; Babiarz, C. L.; Beaty, K. G.; Bodaly, R. A. D.; Branfireun, B. A.; Gilmour, C. C.; Graydon, J. A.; Hall, B. D.; Harris, R. C.; Heyes, A.; Hintelmann, H.; Hurley, J. P.; Kelly, C. A.; Krabbenhoft, D. P.; Lindberg, S. E.; Mason, R. P.; Paterson, M. J.; Podemski, C. L.; Sandilands, K. A.; Southworth, G. R.; St Louis, V. L.; Tate, L. S.; Tate, M. T. Experimental Evidence for Recovery of Mercury-Contaminated Fish Populations. *Nature* **2022**, *601*, 74−78.

(9) Bergamaschi, B. A.; Krabbenhoft, D. P.; Aiken, G. R.; Patino, E.; Rumbold, D. G.; Orem, W. H. Tidally Driven Export of Dissolved Organic Carbon, Total Mercury, and Methylmercury from a Mangrove-Dominated Estuary. *Environ. Sci. Technol.* **2012**, *46*, 1371−1378.

(10) Gilmour, C. C.; Riedel, G. S.; Ederington, M. C.; Bell, J. T.; Gill, G.; Stordal, M.; Stordal, M. C. Methylmercury Concentrations and Production Rates across a Trophic Gradient in the Northern Everglades. *Biogeochemistry* **1998**, *40*, 327−345.

(11) Orem, W. H.; Fitz, C.; Krabbenhoft, D. P.; Poulin, B. A.; Varonka, M. S.; Aiken, G. R. Ecosystem-Scale Modeling and Field Observations of Sulfate and Methylmercury Distributions in the Florida Everglades: Responses to Reductions in Sulfate Loading. *Aquat. Geochem.* **2020**, *26*, 191−220.

(12) Hurley, J. P.; Krabbenhoft, D. P.; Cleckner, L. B.; Olson, M. L.; Aiken, G. R.; Rawlik, P. S. System Controls on the Aqueous Distribution of Mercury in the Northern Florida Everglades. *Biogeochemistry* **1998**, *40*, 293−310.

(13) Cleckner, L. B.; Garrison, P. J.; Hurley, J. P.; Olson, M. L.; Krabbenhoft, D. P. Trophic Transfer of Methyl Mercury in the Northern Florida Everglades. *Biogeochemistry* **1998**, *40*, 347−361.

(14) Dittmar, T.; Hertkorn, N.; Kattner, G.; Lara, R. J. Mangroves, a Major Source of Dissolved Organic Carbon to the Oceans. *Global Biogeochem. Cycles* **2006**, *20*, 2570.

(15) Rumbold, D. G.; Lange, T. R.; Richard, D.; DelPizzo, G.; Hass, N. Mercury Biomagnification through Food Webs along a Salinity

Gradient Down-Estuary from a Biological Hotspot. *Estuar. Coast Shelf Sci.* **2018**, *200*, 116−125.
(16) Buchanan, M. K.; Kulp, S.; Strauss, B. Resilience of U.S. Coastal Wetlands to Accelerating Sea Level Rise. *Environ. Res. Commun.* **2022**, *4*, 061001.
(17) Zhao, X.; Rivera-Monroy, V. H.; Wang, H.; Xue, Z. G.; Tsai, C.-F.; Willson, C. S.; Castañeda-Moya, E.; Twilley, R. R. Modeling Soil Porewater Salinity in Mangrove Forests (Everglades, Florida, USA) Impacted by Hydrological Restoration and a Warming Climate. *Ecol. Model.* **2020**, *436*, 109292.
(18) Lagomasino, D.; Fatoyinbo, T.; Castañeda-Moya, E.; Cook, B. D.; Montesano, P. M.; Neigh, C. S. R.; Corp, L. A.; Ott, L. E.; Chavez, S.; Morton, D. C. Storm Surge and Ponding Explain Mangrove Dieback in Southwest Florida Following Hurricane Irma. *Nat. Commun.* **2021**, *12*, 4003.
(19) Parks, J. M.; Johs, A.; Podar, M.; Bridou, R.; Hurt, R. A.; Smith, S. D.; Tomanicek, S. J.; Qian, Y.; Brown, S. D.; Brandt, C. C.; Palumbo, A. V.; Smith, J. C.; Wall, J. D.; Elias, D. A.; Liang, L. The Genetic Basis for Bacterial Mercury Methylation. *Science* **2013**, *339*, 1332−1335.
(20) Poulin, B. A.; Ryan, J. N.; Tate, M. T.; Krabbenhoft, D. P.; Hines, M. E.; Barkay, T.; Schaefer, J.; Aiken, G. R. Geochemical Factors Controlling Dissolved Elemental Mercury and Methylmercury Formation in Alaskan Wetlands of Varying Trophic Status. *Environ. Sci. Technol.* **2019**, *53*, 6203−6213.
(21) St Louis, V. L.; Rudd, J. W. M.; Kelly, C. A.; Beaty, K. G.; Flett, R. J.; Roulet, N. T. Production and Loss of Methylmercury and Loss of Total Mercury from Boreal Forest Catchments Containing Different Types of Wetlands. *Environ. Sci. Technol.* **1996**, *30*, 2719−2729.
(22) Mitchell, C. P. J.; Branfireun, B. A.; Kolka, R. K. Spatial Characteristics of Net Methylmercury Production Hot Spots in Peatlands. *Environ. Sci. Technol.* **2008**, *42*, 1010−1016.
(23) Janssen, S. E.; Tate, M. T.; Poulin, B. A.; Krabbenhoft, D. P.; DeWild, J. F.; Ogorek, J. M.; Varonka, M. S.; Orem, W. H.; Kline, J. L. Decadal Trends of Mercury Cycling and Bioaccumulation within Everglades National Park. *Sci. Total Environ.* **2022**, *838*, 156031.
(24) Mitchell, C. P. J.; Gilmour, C. C. Methylmercury Production in a Chesapeake Bay Salt Marsh. *J. Geophys. Res.* **2008**, *113*, G00C04.
(25) Bae, H.-S.; Dierberg, F. E.; Ogram, A. Syntrophs Dominate Sequences Associated with the Mercury Methylation-Related Gene HgcA in the Water Conservation Areas of the Florida Everglades. *Appl. Environ. Microbiol.* **2014**, *80*, 6517−6526.
(26) Arndt, S.; Jørgensen, B. B.; LaRowe, D. E.; Middelburg, J. J.; Pancost, R. D.; Regnier, P. Quantifying the Degradation of Organic Matter in Marine Sediments: A Review and Synthesis. *Earth Sci. Rev.* **2013**, *123*, 53−86.
(27) Yu, R. Q.; Reinfelder, J. R.; Hines, M. E.; Barkay, T. Syntrophic Pathways for Microbial Mercury Methylation. *ISME J.* **2018**, *12*, 1826−1835.
(28) Luek, J. L.; Thompson, K. E.; Larsen, R. K.; Heyes, A.; Gonsior, M. Sulfate Reduction in Sediments Produces High Levels of Chromophoric Dissolved Organic Matter. *Sci. Rep.* **2017**, *7*, 8829.
(29) Aiken, G. R.; Gilmour, C. C.; Krabbenhoft, D. P.; Orem, W. Dissolved Organic Matter in the Florida Everglades: Implications for Ecosystem Restoration. *Crit. Rev. Environ. Sci. Technol.* **2011**, *41*, 217−248.
(30) Haitzer, M.; Aiken, G. R.; Ryan, J. N. Binding of Mercury(II) to Dissolved Organic Matter: The Role of the Mercury-to-DOM Concentration Ratio. *Environ. Sci. Technol.* **2002**, *36*, 3564−3570.
(31) Gerbig, C. A.; Kim, C. S.; Stegemeier, J. P.; Ryan, J. N.; Aiken, G. R. Formation of Nanocolloidal Metacinnabar in Mercury-DOM-Sulfide Systems. *Environ. Sci. Technol.* **2011**, *45*, 9180−9187.
(32) Poulin, B. A.; Gerbig, C. A.; Kim, C. S.; Stegemeier, J. P.; Ryan, J. N.; Aiken, G. R. Effects of Sulfide Concentration and Dissolved Organic Matter Characteristics on the Structure of Nanocolloidal Metacinnabar. *Environ. Sci. Technol.* **2017**, *51*, 13133−13142.
(33) Graham, A. M.; Aiken, G. R.; Gilmour, C. C. Effect of Dissolved Organic Matter Source and Character on Microbial Hg Methylation in Hg-S-DOM Solutions. *Environ. Sci. Technol.* **2013**, *47*, 5746−5754.
(34) Graham, A. M.; Aiken, G. R.; Gilmour, C. C. Dissolved Organic Matter Enhances Microbial Mercury Methylation under Sulfidic Conditions. *Environ. Sci. Technol.* **2012**, *46*, 2715−2723.
(35) Poulin, B. A.; Ryan, J. N.; Nagy, K. L.; Stubbins, A.; Dittmar, T.; Orem, W.; Krabbenhoft, D. P.; Aiken, G. R. Spatial Dependence of Reduced Sulfur in Everglades Dissolved Organic Matter Controlled by Sulfate Enrichment. *Environ. Sci. Technol.* **2017**, *51*, 3630−3639.
(36) Graham, A. M.; Cameron-Burr, K. T.; Hajic, H. A.; Lee, C.; Msekela, D.; Gilmour, C. C. Sulfurization of Dissolved Organic Matter Increases Hg-Sulfide-Dissolved Organic Matter Bioavailability to a Hg-Methylating Bacterium. *Environ. Sci. Technol.* **2017**, *51*, 9080−9088.
(37) Weishaar, J. L.; Aiken, G. R.; Bergamaschi, B. A.; Fram, M. S.; Fujii, R.; Mopper, K. Evaluation of Specific Ultraviolet Absorbance as an Indicator of the Chemical Composition and Reactivity of Dissolved Organic Carbon. *Environ. Sci. Technol.* **2003**, *37*, 4702−4708.
(38) Åkerblom, S.; Nilsson, M. B.; Skyllberg, U.; Björn, E.; Jonsson, S.; Ranneby, B.; Bishop, K. Formation and Mobilization of Methylmercury across Natural and Experimental Sulfur Deposition Gradients. *Environ. Pollut.* **2020**, *263*, 114398.
(39) Mason, R. P.; Reinfelder, J. R.; Morel, F. M. M. Uptake, Toxicity, and Trophic Transfer of Mercury in a Coastal Diatom. *Environ. Sci. Technol.* **1996**, *30*, 1835−1845.
(40) Moye, H. A.; Miles, C. J.; Phlips, E. J.; Sargent, B.; Merritt, K. K. Kinetics and Uptake Mechanisms for Monomethylmercury between Freshwater Algae and Water. *Environ. Sci. Technol.* **2002**, *36*, 3550−3555.
(41) Luengen, A. C.; Fisher, N. S.; Bergamaschi, B. A. Dissolved Organic Matter Reduces Algal Accumulation of Methylmercury. *Environ. Toxicol. Chem.* **2012**, *31*, 1712−1719.
(42) Zhang, K. Analysis of Non-Linear Inundation from Sea-Level Rise Using LIDAR Data: A Case Study for South Florida. *Clim. Change* **2011**, *106*, 537−565.
(43) Park, J.; Stabenau, E.; Redwine, J.; Kotun, K. South Florida's Encroachment of the Sea and Environmental Transformation over the 21st Century. *J. Mar. Sci. Eng.* **2017**, *5*, 31.
(44) Damseaux, F.; Kiszka, J. J.; Heithaus, M. R.; Scholl, G.; Eppe, G.; Thomé, J. P.; Lewis, J.; Hao, W.; Fontaine, M. C.; Das, K. Spatial Variation in the Accumulation of POPs and Mercury in Bottlenose Dolphins of the Lower Florida Keys and the Coastal Everglades (South Florida). *Environ. Pollut.* **2017**, *220*, 577−587.
(45) Orem, W.; Gilmour, C.; Axelrad, D.; Krabbenhoft, D.; Scheidt, D.; Kalla, P.; McCormick, P.; Gabriel, M.; Aiken, G. Sulfur in the South Florida Ecosystem: Distribution, Sources, Biogeochemistry, Impacts, and Management for Restoration. *Crit. Rev. Environ. Sci. Technol.* **2011**, *41*, 249−288.
(46) Tate, M. T.; DeWild, J. F.; Ogorek, J. M.; Janssen, S. E.; Krabbenhoft, D. P.; Poulin, B. A.; Breitmeyer, S. E.; Aiken, G. R.; Orem, W. H.; Varonka, M. S. *Chemical Characterization of Water, Sediments, and Fish from Water Conservation Areas and Canals of the Florida Everglades (USA), 2012 to 2019*; U.S. Geological Survey Data Release, 2023, DOI: 10.5066/P976EGIX.
(47) Schall, T. N.; Ruiz, P. L.; Rutchey, K.; Irving, C.; McFee, D.; Caldecutt, K.; Maholland, B.; Bogina, V.; McCoy, C.; Shamblin, R. B.; Whelan, K. R. T. *The Everglades National Park and Big Cypress National Preserve Vegetation Mapping Project: Interim Report-Shark River Slough/Long Pine Key (Region 1), Everglades National Park*: Jacksonville District, Jacksonville, FL, 2020.
(48) Wilson, B. J.; Servais, S.; Mazzei, V.; Kominoski, J. S.; Hu, M.; Davis, S. E.; Gaiser, E.; Sklar, F.; Bauman, L.; Kelly, S.; Madden, C.; Richards, J.; Rudnick, D.; Stachelek, J.; Troxler, T. G. Salinity Pulses Interact with Seasonal Dry-down to Increase Ecosystem Carbon Loss in Marshes of the Florida Everglades. *Ecol. Appl.* **2018**, *28*, 2092−2108.
(49) Chambers, L. G.; Reddy, K. R.; Osborne, T. Z. Short-Term Response of Carbon Cycling to Salinity Pulses in a Freshwater Wetland. *Soil Sci. Soc. Am. J.* **2011**, *75*, 2000−2007.
(50) Servais, S.; Kominoski, J. S.; Charles, S. P.; Gaiser, E. E.; Mazzei, V.; Troxler, T. G.; Wilson, B. J. Saltwater Intrusion and Soil Carbon Loss: Testing Effects of Salinity and Phosphorus Loading on Microbial

Functions in Experimental Freshwater Wetlands. *Geoderma* **2019**, *337*, 1291−1300.
(51) Gaiser, E.; Childers, D.; Travieso, R. *Water Quality Data (Grab Samples) from the Shark River Slough, Everglades National Park (FCE LTER), Florida, USA, May 2001-Ongoing Ver 16*; Environmental Data Initiative, 2022.
(52) Castaneda, E.; Rivera-Monroy, V. *Abiotic Monitoring of Physical Characteristics in Porewaters and Surface Waters of Mangrove Forests from the Shark River Slough and Taylor Slough, Everglades National Park (FCE LTER), South Florida, USA, December 2000-Ongoing*; Environmental Data Initiative, 2023.
(53) Aiken, G. R.; McKnight, D. M.; Thorn, K. A.; Thurman, E. M. Isolation of Hydrophilic Organic Acids from Water Using Nonionic Macroporous Resins. *Org. Geochem.* **1992**, *18*, 567−573.
(54) Pucher, M.; Wünsch, U.; Weigelhofer, G.; Murphy, K.; Hein, T.; Graeber, D. StaRdom: Versatile Software for Analyzing Spectroscopic Data of Dissolved Organic Matter in R. *Water* **2019**, *11*, 2366.
(55) Helms, J. R.; Stubbins, A.; Ritchie, J. D.; Minor, E. C.; Kieber, D. J.; Mopper, K. Absorption Spectral Slopes and Slope Ratios as Indicators of Molecular Weight, Source, and Photobleaching of Chromophoric Dissolved Organic Matter. *Limnol. Oceanogr.* **2008**, *53*, 955−969.
(56) Cook, B. A.; Janssen, S. E.; Tate, M. T.; Peterson, B. D.; Poulin, B. A. *Mercury Methylation Assay Along a Salinity Gradient in Coastal Peat Soils in the Florida Everglades*, U.S. Geological Survey Data Release, 2024, DOI: 10.5066/P139NMHU.
(57) NIST. *NIST Standard Reference Database 46, Ver 4.0. Critical Stability Constants of Metal Complexes Database*; National Institute of Standards and Technology, 1997.
(58) NIST. *NIST Standard Reference Database 13, Ver 1. 0. NIST JANAF Thermochemical Tables*; National Institute of Standards and Technology, 1985.
(59) Davison, W. The Solubility of Iron Sulphides in Synthetic and Natural Waters at Ambient Temperature. *Aquat. Sci.* **1991**, *53*, 309−329.
(60) Nordstrom, D. K.; Plummer, L. N.; Langmuir, D.; Busenberg, E.; May, H. M.; Jones, B. F.; Parkhurst, D. L. Revised Chemical Equilibrium Data for Major Water-Mineral Reactions and Their Limitations. In *Chemical Modeling of Aqueous Systems II*; ACS Symposium Series; American Chemical Society, 1990; Vol. *416*, pp 398−413.
(61) Drott, A.; Björn, E.; Bouchet, S.; Skyllberg, U. Refining Thermodynamic Constants for Mercury(II)-Sulfides in Equilibrium with Metacinnabar at Sub-Micromolar Aqueous Sulfide Concentrations. *Environ. Sci. Technol.* **2013**, *47*, 4197−4203.
(62) Haitzer, M.; Aiken, G. R.; Ryan, J. N. Binding of Mercury(II) to Aquatic Humic Substances: Influence of PH and Source of Humic Substances. *Environ. Sci. Technol.* **2003**, *37*, 2436−2441.
(63) Amirbahman, A.; Reid, A. L.; Haines, T. a.; Kahl, J. S.; Arnold, C. Association of Methylmercury with Dissolved Humic Acids. *Environ. Sci. Technol.* **2002**, *36*, 690−695.
(64) Zeng, T.; Arnold, W. A.; Toner, B. M. Microscale Characterization of Sulfur Speciation in Lake Sediments. *Environ. Sci. Technol.* **2013**, *47*, 1287−1296.
(65) Bates, A. L.; Spiker, E. C.; Holmes, C. W. Speciation and Isotopic Composition of Sedimentary Sulfur in the Everglades, Florida, USA. *Chem. Geol.* **1998**, *146*, 155−170.
(66) Gilmour, C.; Krabbenhoft, D.; Orem, W.; Aiken, G. *Appendix 2B-1%: Influence of Drying and Rewetting on Mercury and Sulfur Cycling in Everglades and STA Soils*, 2004 Everglades consolidated report for the South Florida Water Management District: West Palm Beach, FL, 2004.
(67) Sleighter, R. L.; Chin, Y.-P.; Arnold, W. A.; Hatcher, P. G.; McCabe, A. J.; McAdams, B. C.; Wallace, G. C. Evidence of Incorporation of Abiotic S and N into Prairie Wetland Dissolved Organic Matter. *Environ. Sci. Technol. Lett.* **2014**, *1*, 345−350.
(68) Chambers, L. G.; Davis, S. E.; Troxler, T.; Boyer, J. N.; Downey-Wall, A.; Scinto, L. J. Biogeochemical Effects of Simulated Sea Level Rise on Carbon Loss in an Everglades Mangrove Peat Soil. *Hydrobiologia* **2014**, *726*, 195−211.
(69) Weston, N. B.; Vile, M. A.; Neubauer, S. C.; Velinsky, D. J. Accelerated Microbial Organic Matter Mineralization Following Salt-Water Intrusion into Tidal Freshwater Marsh Soils. *Biogeochemistry* **2011**, *102*, 135−151.
(70) Weston, N. B.; Dixon, R. E.; Joye, S. B. Ramifications of Increased Salinity in Tidal Freshwater Sediments: Geochemistry and Microbial Pathways of Organic Matter Mineralization. *J. Geophys. Res.: Biogeosci.* **2006**, *111*, G01009.
(71) Sholkovitz, E. R. Flocculation of Dissolved Organic and Inorganic Matter during the Mixing of River Water and Seawater. *Geochim. Cosmochim. Acta* **1976**, *40*, 831−845.
(72) Poulin, B. A.; Aiken, G. R.; Nagy, K. L.; Manceau, A.; Krabbenhoft, D. P.; Ryan, J. N. Mercury Transformation and Release Differs with Depth and Time in a Contaminated Riparian Soil during Simulated Flooding. *Geochim. Cosmochim. Acta* **2016**, *176*, 118−138.
(73) Weber, F. A.; Voegelin, A.; Kretzschmar, R. Multi-Metal Contaminant Dynamics in Temporarily Flooded Soil under Sulfate Limitation. *Geochim. Cosmochim. Acta* **2009**, *73*, 5513−5527.
(74) D'Andrilli, J.; Junker, J. R.; Smith, H. J.; Scholl, E. A.; Foreman, C. M. DOM Composition Alters Ecosystem Function during Microbial Processing of Isolated Sources. *Biogeochemistry* **2019**, *142*, 281−298.
(75) Herzog, S. D.; Persson, P.; Kvashnina, K.; Kritzberg, E. S. Organic Iron Complexes Enhance Iron Transport Capacity along Estuarine Salinity Gradients of Baltic Estuaries. *Biogeosciences* **2020**, *17*, 331−344.
(76) Nagy, K. L.; Manceau, A.; Gasper, J. D.; Ryan, J. N.; Aiken, G. R. Metallothionein-like Multinuclear Clusters of Mercury(II) and Sulfur in Peat. *Environ. Sci. Technol.* **2011**, *45*, 7298−7306.
(77) Marvin-DiPasquale, M.; Agee, J.; McGowan, C.; Oremland, R. S.; Thomas, M.; Krabbenhoft, D.; Gilmour, C. C. Methyl-Mercury Degradation Pathways: A Comparison among Three Mercury-Impacted Ecosystems. *Environ. Sci. Technol.* **2000**, *34*, 4908−4916.
(78) Cleckner, L. B.; Gilmour, C. C.; Hurley, J. P.; Krabbenhoft, D. P. Mercury Methylation in Periphyton of the Florida Everglades. *Limnol Oceanogr* **1999**, *44*, 1815−1825.
(79) Qian, J.; Skyllberg, U.; Frech, W.; Bleam, W. F.; Bloom, P. R.; Petit, P. E. Bonding of Methyl Mercury to Reduced Sulfur Groups in Soil and Stream Organic Matter as Determined by X-Ray Absorption Spectroscopy and Binding Affinity Studies. *Geochim. Cosmochim. Acta* **2002**, *66*, 3873−3885.
(80) Peterson, B. D.; Poulin, B. A.; Krabbenhoft, D. P.; Tate, M. T.; Baldwin, A. K.; Naymik, J.; Gastelecutto, N.; McMahon, K. D. Metabolically Diverse Microorganisms Mediate Methylmercury Formation under Nitrate-Reducing Conditions in a Dynamic Hydroelectric Reservoir. *ISME J.* **2023**, *17* (10), 1705−1718.
(81) Peterson, B. D.; McDaniel, E. A.; Schmidt, A. G.; Lepak, R. F.; Janssen, S. E.; Tran, P. Q.; Marick, R. A.; Ogorek, J. M.; Dewild, J. F.; Krabbenhoft, D. P.; McMahon, K. D. Mercury Methylation Genes Identified across Diverse Anaerobic Microbial Guilds in a Eutrophic Sulfate-Enriched Lake. *Environ. Sci. Technol.* **2020**, *54*, 15840−15851.
(82) Jones, D. S.; Walker, G. M.; Johnson, N. W.; Mitchell, C. P. J.; Coleman Wasik, J. K.; Bailey, J. V. Molecular Evidence for Novel Mercury Methylating Microorganisms in Sulfate-Impacted Lakes. *ISME J.* **2019**, *13*, 1659−1675.
(83) Chambers, L. G.; Steinmuller, H. E.; Breithaupt, J. L. Toward a Mechanistic Understanding of "Peat Collapse" and Its Potential Contribution to Coastal Wetland Loss. *Ecology* **2019**, *100*, No. e02720.
(84) McCarter, C. P. R.; Sebestyen, S. D.; Coleman Wasik, J. K.; Engstrom, D. R.; Kolka, R. K.; Jeremiason, J. D.; Swain, E. B.; Monson, B. A.; Branfireun, B. A.; Balogh, S. J.; Nater, E. A.; Eggert, S. L.; Ning, P.; Mitchell, C. P. J. Long-Term Experimental Manipulation of Atmospheric Sulfate Deposition to a Peatland: Response of Methylmercury and Related Solute Export in Streamwater. *Environ. Sci. Technol.* **2022**, *56*, 17615−17625.
(85) Mitchell, C. P. J.; Branfireun, B. A.; Kolka, R. K. Assessing Sulfate and Carbon Controls on Net Methylmercury Production in Peatlands: An in Situ Mesocosm Approach. *Appl. Geochem.* **2008**, *23*, 503−518.
(86) Chambers, L. G.; Guevara, R.; Boyer, J. N.; Troxler, T. G.; Davis, S. E. Effects of Salinity and Inundation on Microbial Community

Structure and Function in a Mangrove Peat Soil. *Wetlands* **2016**, *36*, 361−371.
(87) Ulus, Y.; Tsui, M. T.-K.; Sakar, A.; Nyarko, P.; Aitmbarek, N. B.; Ardón, M.; Chow, A. T. Declines of Methylmercury along a Salinity Gradient in a Low-Lying Coastal Wetland Ecosystem at South Carolina, USA. *Chemosphere* **2022**, *308*, 136310.

https://doi.org/10.1021/acsearthspacechem.4c00124
ACS Earth Space Chem. XXXX, XXX, XXX−XXX